Biodistribution of X-Ray Iodinated Contrast Agent in Nano-Emulsions Is Controlled by the Chemical Nature of the Oily Core

Mohamed F. Attia,[†,‡] Nicolas Anton,[*,†,‡] Manuela Chiper,[†,‡] Roman Akasov,[†,‡,§] Halina Anton,[†,⊥] Nadia Messaddeq,[∥] Sylvie Fournel,[†,‡] Andrey S. Klymchenko,[†,⊥] Yves Mély,[†,⊥] and Thierry F. Vandamme[†,‡]

[†]University of Strasbourg, Faculty of Pharmacy, 74 route du Rhin, 67401 Illkirch Cedex, France, [‡]CNRS UMR 7199, Laboratoire de Conception et Application de Molécules Bioactives, University of Strasbourg, 74 route du Rhin, 67401 Illkirch Cedex, France, [§]Shemyakin-Ovchinnikov Institute of Bioorganic Chemistry, Russian Academy of Sciences, Miklukho-Maklaya Str., 16/10117997, Moscow, Russia, [⊥]CNRS UMR 7213, Laboratoire de Biophotonique et Pharmacologie, University of Strasbourg, 74 route du Rhin, 67401 Illkirch Cedex, France, and [∥]IGBMC (Institut de Génétique et de Biologie Moléculaire et Cellulaire), Inserm U964, CNRS UMR7104, Université de Strasbourg, 1 rue Laurent Fries, 67404 Illkirch, France

ABSTRACT In this study, we investigated the role of the chemical nature of the oil droplet core of nano-emulsions used as contrast agents for X-ray imaging on their pharmacokinetics and biodistribution. To this end, we formulated PEGylated nano-emulsions with two iodinated oils (*i.e.*, iodinated monoglyceride and iodinated castor oil) and compared them with another iodinated nano-emulsion based on iodinated vitamin E. By using dynamic light scattering and transmission electron microscopy, the three iodinated nano-emulsions were found to exhibit comparable morphologies, size, and surface composition. Furthermore, they were shown to be endowed with very high iodine concentration, which leads to stronger X-ray attenuation properties as compared to the commercial iodinated nano-emulsion Fenestra VC. The three nano-emulsions were i.v. administered in mice and monitored by microcomputed tomography (micro-CT). They showed high contrast enhancement in blood with similar half-life around 6 h but very different accumulation sites. While iodinated monoglycerides exhibited low accumulation in liver and spleen, high accumulation in spleen was observed for iodinated castor oil and in liver for vitamin E. These data clearly highlighted the important role of the oil composition of the nano-emulsion core to obtain strong X-ray contrast enhancement in specific targets such as liver, spleen, or only blood. These differences in biodistribution were partly attributed to differences in the uptake of the nanodroplets by the macrophages *in vitro*. Another key feature of these nano-emulsions is their long half-elimination time (several weeks), which offers sufficient retention for micro-CT imaging. This work paves the way for the design of nanoparticulate contrast agents for X-ray imaging of selected organs.

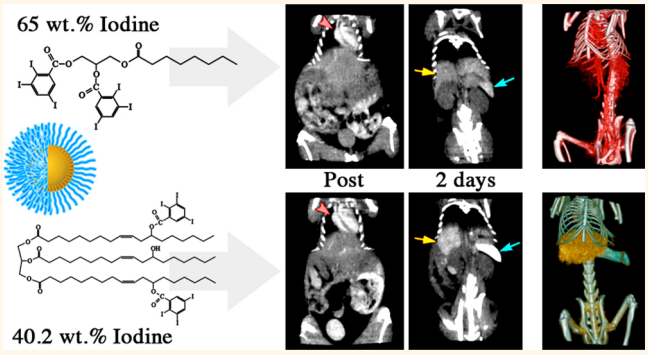

KEYWORDS: X-ray imaging · micro-CT · contrast agent · nano-emulsion · targeting

During the past decade, X-ray micro-computed tomography (micro-CT) emerged as a key imaging modality for biomedical research. Micro-CT provides high-resolution, noninvasive, structural, and functional imaging at low cost compared to magnetic resonance imaging and without tedious experimental protocols compared to nuclear imaging.[1,2] However, in spite of the strong progress recently achieved on microscanners, with a notable reduction of the voxel size down to 10 μm or acquisition times lower than 5 min, their use is still limited by the poor efficiency of the available contrast agents. Indeed, in the absence of contrast agents, micro-CT only allows differentiating bones (electron-dense) from soft tissues including organs or fluids.[3] Therefore, micro-CT is often used in association with another imaging modality (like single-photon emission computed tomography, SPECT) in order to help locate the SPECT signal within the whole animal body, such as for tumor location. The possibilities offered by X-ray scanners are largely improved by using electron-dense contrast

* Address correspondence to nanton@unistra.fr.

Received for review July 18, 2014 and accepted October 3, 2014.

Published online October 04, 2014
10.1021/nn503973z

© 2014 American Chemical Society

agents, which allow direct visualization of the biological compartments in which they accumulate,[3,4] providing thus structural and potentially functional, noninvasive imaging with high resolution. As discussed in previous reports.[1,2,5] there are fundamental differences between contrast agents designed for clinical X-ray scanners and those formulated for micro-CT. Clinical contrast agents were designed as small hydrophilic iodinated molecules, which are excreted by the kidney only a few minutes after i.v. administration. Since clinical agents were developed before modern and fast scanners were available, considerable investments were made by industry to adapt the scanners to the contrast agents and make them fast. However, these contrast agents are less appropriate for micro-CT since their renal clearance kinetics is comparable to the image acquisition times of this modality. Therefore, high doses or multiple administrations are needed to improve the contrast, which results in significant side effects, like nephropathy, acute kidney injury, or renal failure. With the objective of using micro-CT for imaging soft tissues and organs with pathologies like tumors, new contrast agents were developed in the past decade. To slow down or avoid their renal elimination, the idea was to increase the size of the contrast agents above the 50−100 nm diameter of the glomerulus pores.[2,5−11] To this end, several nanoparticle systems were developed in the form of iodinated liposomes, polymeric micelles, dendrimers, inorganic nanoparticles (based on gold, bismuth, silver, tungsten),[4,12] and iodinated nano-emulsions.[2,5] The main constraint, directly linked to the contrast enhancement, is the concentration of heavy atoms, which has to be as high as possible. Moreover, the toxicity of the nanoparticles should be as low as possible, which depends on the chemical nature of the nanoparticle components (lipid, polymer, inorganic compounds) and the loading dose required for obtaining a good contrast. Finally, the last important aspect of the formulation of nanoparticulate CT contrast agent concerns their surface properties that can strongly influence their pharmacokinetics and/or biodistribution after injection. As a rule, decorating the nanoparticle surface with polyethylene glycol (PEG) increases their circulation time in the bloodstream.[13−15] Actually, long circulating systems (also called "blood pool contrast agents") not only allow performing angiography with micro-CT but also are used for the formulation of targeted systems, based on the fact that the longer the vascular circulation, the longer the time in contact with the potential targets in the whole body.[2] In general, innovation in CT contrast agents is based on already well-known scaffolds[8,16,17] such as gold and iodinated liposomes, through improved formulation, chemical nature, and surface functionalization.

An overview of the recent literature on micro-CT nanoparticulate contrast agents shows that the major difficulty encountered in designing these contrast agents comes from the need to concentrate the contrasting atoms within the nanoparticles,[2,4] so that nontoxic doses of nanoparticles could be injected. Only few families of nanoparticles allow formulating contrast agents at high concentrations in heavy atoms, representative examples being inorganic particles based on elements like gold,[18−22] bismuth,[23] or tantalum[24] and iodinated lipid-based nanoparticles like liposomes and nano-emulsions. In our previous studies,[5,25] we have shown that iodinated nano-emulsions appear as one of the best compromises to provide very high contrast without toxicity. Compared to inorganic nanoparticles,[4] lipid nano-emulsions are easier to synthesize and formulate, enable complete clearance from the body, and offer the possibility to use the oily core of the nanodroplets as a reservoir for drugs. In addition, micro-CT allows monitoring with time the biodistribution of the contrast agent in the living animal. This is fundamental to understand the influence of the physicochemical properties of the formulations on their *in vivo* biodistribution and pharmacokinetics, in order to optimize the processes and adapt the contrast agents to the imaging targets. Moreover, coencapsulating the active principle in the oily core of the iodinated nano-emulsion droplets, coupled with the possibility to follow up the *in vivo* biodistribution, offers new therapeutic potentials like "online" monitoring and quantification of the actual dosage of active principles brought on various sites.

The objective of the present study was to investigate how the composition of nano-emulsions (*i.e.*, the chemical nature of the iodinated lipid core of droplets) can control the biodistribution of the contrast agent and thus the contrast enhancement. To this end, two new iodinated lipids were synthesized, namely, iodinated monoglycerides and iodinated castor oil (structures are shown in Figure 1a), and formulated as nano-emulsions by the spontaneous emulsification method (Figure 1b). Formulation processes were optimized, and both new iodinated nano-emulsions were characterized by dynamic light scattering (DLS), transmission electron microcopy (TEM), and by MTT cell viability assays *in vitro*. Then, *in vivo* contrasting properties, biodistribution, and pharmacokinetics were evaluated in mice with micro-CT and followed up over 2 months. The efficiency of the accumulation in liver, spleen, and kidneys, as a function of the nature of iodinated oil, was assessed and compared with that of nano-emulsions prepared with iodinated vitamin E. While kinetics of blood clearance appeared similar between the two types of oils, the accumulations in organs (liver, spleen) after blood clearance were found to significantly differ.

RESULTS AND DISCUSSION

After synthesis and purification, the iodinated oils were formulated into nano-emulsions following the same protocol. Process optimizations were carried out

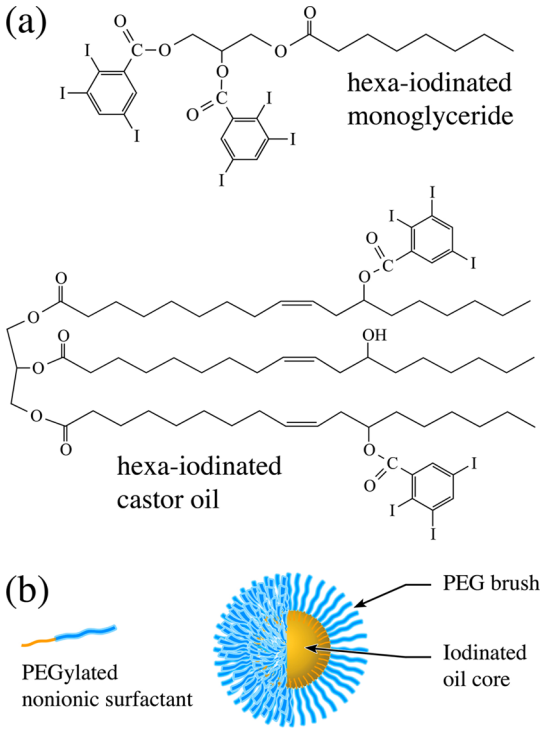

Figure 1. (a) Chemical structures of iodinated monoglyceride and castor oil. (b) Schematic representation of an iodinated nano-emulsion droplet.

by following the impact of the surfactant amount (SOR) on the droplet sizes (hydrodynamic diameter). This point is illustrated in Figure $2a_1$,b_1, both comparing emulsification process before (open symbols) and after (filled symbols) oil iodination for (a) monoglyceride and (b) castor oil.

The trend generally observed in such diagrams, and globally confirmed here, is a decrease in the droplet size with increasing surfactant amounts. We have previously shown[26] that spontaneous nanoemulsification is induced by the sudden solubilization of the surfactant by the aqueous phase, which breaks up the oil/surfactant phase into oil droplets dispersed in water. The process is governed by the surfactant affinities (*i.e.*, solubility) for the oil and water phases. Surfactants have to be first soluble in oil to ensure a perfect homogeneity (helped by temperature since non-ionic PEGylated surfactants are thermosensitive) and then even more soluble in water to ensure fast water penetration and droplet breaking up. In Figure $2a_1$,b_1, emulsification appears less efficient for non-iodinated oils, probably due to their higher hydrophobicity as compared to non-iodinated oils that decrease the solubility of surfactants and thus slow down the water breaking-up step. Moreover, the viscosity appears much higher for iodinated than for non-iodinated oils, which may further contribute to slow the water fractionation process and increase the droplet size. As a result, in the conditions indicated in gray in Figure $2a_1$,b_1, emulsification of iodinated oils is impeded and nano-emulsions do not form. In contrast, iodinated nanoformulations with droplets of small size and narrow PDI were obtained for high SOR values. However, as SOR increases, the iodine content of the droplets decreases as a result of their decreased size. As a consequence, formulations selected for contrast agent applications should be a compromise to ensure that droplet size and PDI are compatible with i.v. administration and sufficient iodine content for getting optimal contrast in imaging. The selected formulations are indicated by arrows in Figure $2a_1$,b_1; they correspond to SOR values of 60 and 65%, respectively, for iodinated monoglyceride and iodinated castor oil. The size distributions of the two formulations are reported in Figure $2a_2$,b_2, while their TEM images are given in Figure $2a_3$,b_3. For iodinated monoglycerides, a narrow log-normal size distribution of the nanoparticles, centered at 130 nm, is observed. This narrow size distribution is confirmed by TEM, showing homogeneous droplets. For iodinated castor oil, the log-normal size distribution is also narrow, being centered at 200 nm and largely overlapping the size distribution of the former nanoparticles. Thus, both formulations provide particles of similar size. The TEM pictures of iodinated castor oil nanodroplets confirmed the homogeneity of the spherical dispersion of droplets (Figure $2b_3$). However, at the highest magnification, in contrast with Figure $2a_3$, a core/shell segregation indicated by arrows was observed. This separation between the oily dense core and the non-ionic surfactant at the interface likely arises from a loss of miscibility between these compounds after the temperature drop during emulsification. This difference in physicochemical properties could also explain the somewhat different dependence of their diameter as a function of the SOR (Figure $2a_1$,b_1). However, it is interesting to note that, in spite of the dramatic changes in the oil properties due to iodination, the spontaneous emulsification process still leads to droplets with good monodispersity.

The strong interest of lipid nano-emulsions comes from their potential to provide nontoxic aqueous dispersions with very high concentrations in iodine. Indeed, the selected nano-emulsions present outstanding amounts in weight of iodine *versus* oils of 64.5 and 40.2% for iodinated monoglyceride and castor oil, respectively. When it is assumed that the amount of surfactant at the nanodroplet interface is negligible compared to the amount of oil in the nanodroplet, similar percentages could be deduced for the iodine content of the nanodroplets. Moreover, an iodine content of 10.3 and 5.6% could be calculated for the whole nano-emulsions (respectively, for monoglyceride and castor oil).

The actual amount of iodine in the formulations was further assessed *in vitro* through their contrasting properties in the micro-CT scanner, by comparison to a

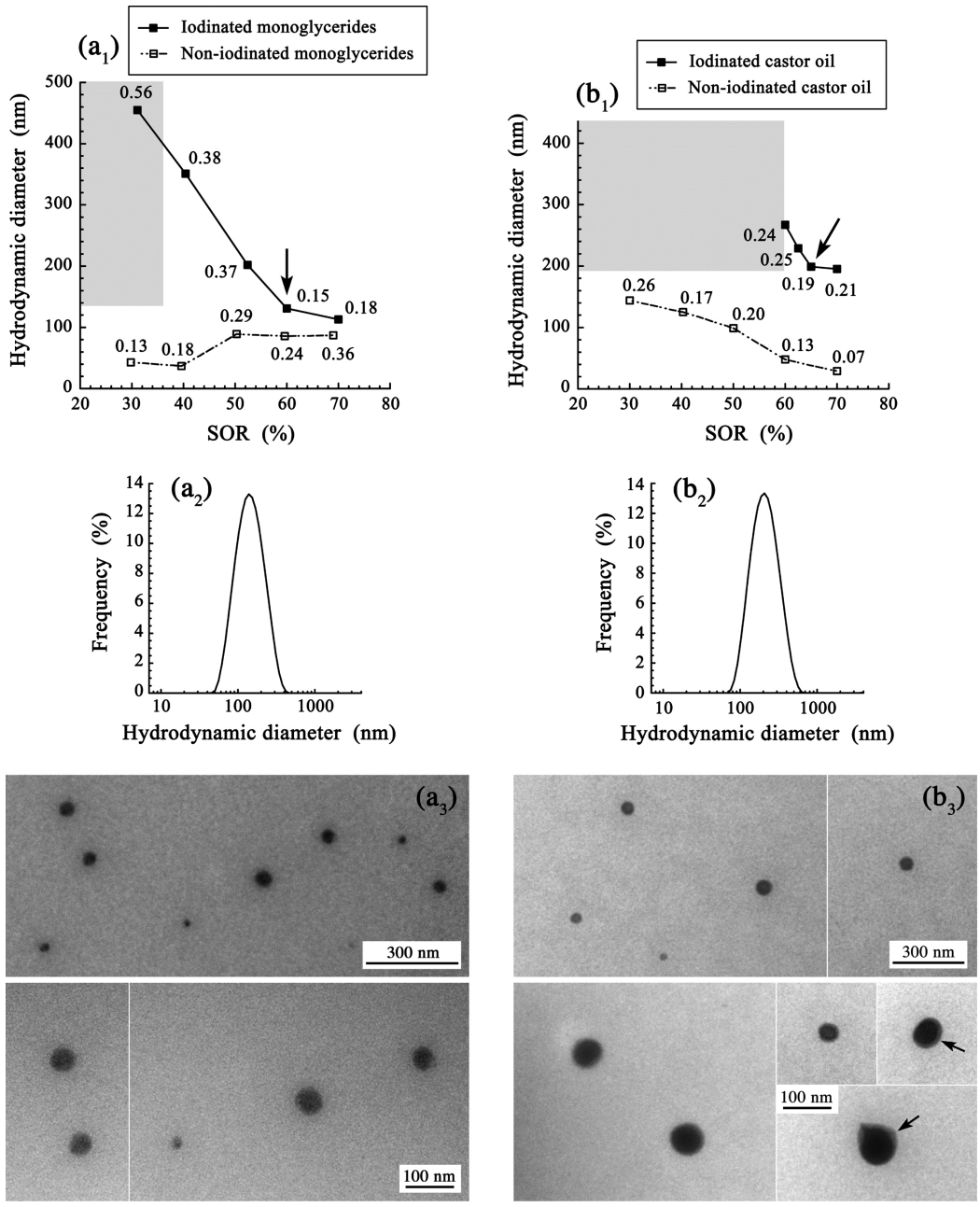

Figure 2. DLS and TEM characterization of nano-emulsions of (a) hexa-iodinated monoglyceride and (b) hexa-iodinated castor oil. (a_1,b_1) Present the impact of the surfactant concentration (SOR = surfactant/(surfactant + oil) weight ratio) on the hydrodynamic size and polydispersity index (PDI, labeled for each point in the graph) measured by DLS. The gray areas show the regions in which nano-emulsions do not form (either size or PDI are too high). The arrows indicate the optimized formulations selected for the *in vivo* studies: SOR = 60% for iodinated monoglycerides, and SOR = 65% for iodinated castor oil. (a_2,b_2) Size distributions of the optimized formulations (corresponding to the arrows in (a_1) and (b_1)). (a_3,b_3) TEM micrographs of nano-emulsions with optimized formulations (corresponding to the arrows in (a_1) and (b_1)).

calibration curve made with iobitridol (XenetiX 300). The results are reported in Figure 3, together with the commercial iodinated nano-emulsion Fenestra VC, and another formulation based on tri-iodinated vitamin E (α-tocopheryl 2,3,5-triiodobenzoate) from our previous work.[5]

As expected, the X-ray attenuation was found to linearly grow with iodine concentration. Quantification from the iobitridol standard gives iodine concentrations of the selected formulations (arrows in Figure 2) of 93.1 mg/mL of iodine for iodinated monoglyceride nano-emulsions and of 76.0 mg/mL of iodine for iodinated castor oil nano-emulsions, in full line with the concentration expected theoretically as calculated from the chemical structure. This high theoretical concentration is thought to play a major role in the signal/noise ratio and the imaging resolution in X-ray scanners. This point has been illustrated recently by the imaging of tumor microvascularization,[8] which is especially challenging. Indeed, the blood pool is the

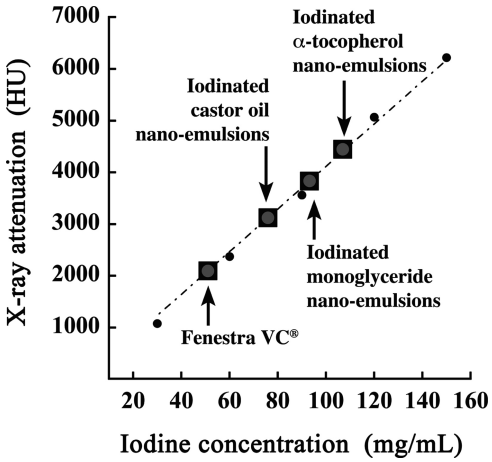

Figure 3. *In vitro* **evaluation of the X-ray attenuation properties of hexa-iodinated monoglyceride and hexa-iodinated castor oil nano-emulsions using a calibration curve made with iobitridol (filled circles). The values of radiopacity of two other iodinated nano-emulsions, namely, iodinated α-tocopherol and Fenestra VC (reproduced with permission from ref 5; copyright 2013 Elsevier), are also reported for comparison.**

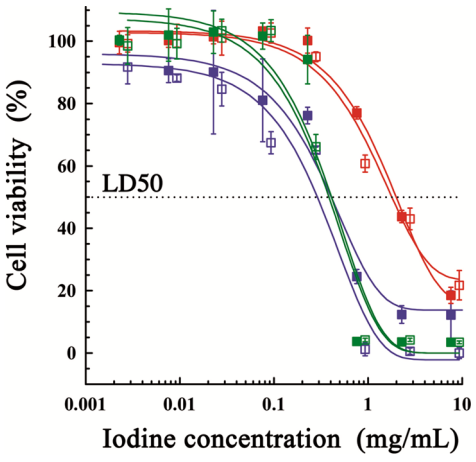

Figure 4. Cytotoxicity MTT experiments. Cells were incubated for 24 h with various concentrations of iodinated nano-emulsions. The nano-emulsion concentrations were expressed in iodine concentrations per mL. Open symbols correspond to iodinated monoglyceride nano-emulsions, and filled symbols correspond to iodinated castor oil nano-emulsions. Blue: HeLa cells. Green: BNL-CL2 hepatocytes. Red: RAW264.7 murine macrophages.

biological compartment with the largest volume, so that dilution of the contrasting atoms will be high, leading to a strong decrease of the signal/noise ratio. An additional difficulty is related to the small size of the capillaries or microvessels, which requires high-resolution imaging. To obtain the required signal-to-noise ratio and resolution, the X-ray attenuation signal was increased by increasing the contrasting properties of the contrast agent, using a liposomal suspension highly concentrated in iodine (around 110 mg/mL of iodine).

Then, *in vitro* toxicity of iodinated nano-emulsion suspensions was assessed by MTT assays after incubation of the nano-emulsions for 24 h with cells at different concentrations (Figure 4). The toxicity was globally similar for iodinated monoglycerides and iodinated castor oil, with LD_{50} values of 0.4 mg/mL of iodine for human cervix epithelial HeLa and mouse hepatocyte BNL-CL2 cells. Toxicity was slightly less for the mouse macrophage cell line RAW264.7 with a LD_{50} around 2 mg/mL of iodine. Considering that the iodinated nano-emulsion suspensions are administered at 7.59 μL/g of mouse for imaging experiments, the corresponding iodine concentration in the animal body (obtained from Figure 3) is 0.67 and 0.57 mg/g of mouse for the iodinated monoglycerides and iodinated castor oil, respectively. Both values are close to the LD_{50} values for HeLa and BNL-CL2 cells, but it has to be kept in mind that the conditions in the MTT assays are more drastic than those *in vivo* because, during the 24 h incubation, the cells are in prolonged contact with the droplets as well as with free surfactants. In contrast, these surfactants are generally rapidly cleared from blood *in vivo*.[25]

Once administered in mice by i.v., the nano-emulsions were immediately spread in the whole animal vasculature. No clinical sign of disorder or toxicity was observed in any mice, during and after injection and through all the experiment duration. The weight of mice was measured and followed all along the micro-CT acquisitions period, that is, 50 days (see Supporting Information), showing fully normal evolution. *In vivo* contrast enhancement induced by these contrast agents is illustrated at different representative acquisition times in Figure 5. Immediately after injection (5 min), a strong contrast enhancement arises in the whole vasculature system, showing a clear delineation of the blood pool. In this early stage after administration, the distribution and contrast enhancements induced by both iodinated formulations appear very similar, as expected from the identical surface composition of both nano-emulsions and their similar iodine concentrations. However, the *in vivo* behaviors of the two nano-emulsions differ when blood clearance mechanisms and elimination begin. This is illustrated at 24 h postinjection, where both nano-emulsions are totally eliminated from the blood pool but accumulate in different organs. The most pronounced difference between the two formulations is observable in the spleen, which shows a strong contrast with liver for the iodinated castor oil but not for the iodinated monoglycerides. Finally, 50 days after injection, the contrast between spleen and liver was dramatically reduced, indicating that iodinated oils are gradually eliminated from the body.

Three-dimensional volume rendering of the blood vessels provided by iodinated monoglyceride nano-emulsions, 5 min after injection, is presented in Figure 6a. The blood compartment in the heart as well as vessels, aortic arch (aar) and thoracic aorta (ta), is clearly visible. Liver irrigation is nicely visible, as well.

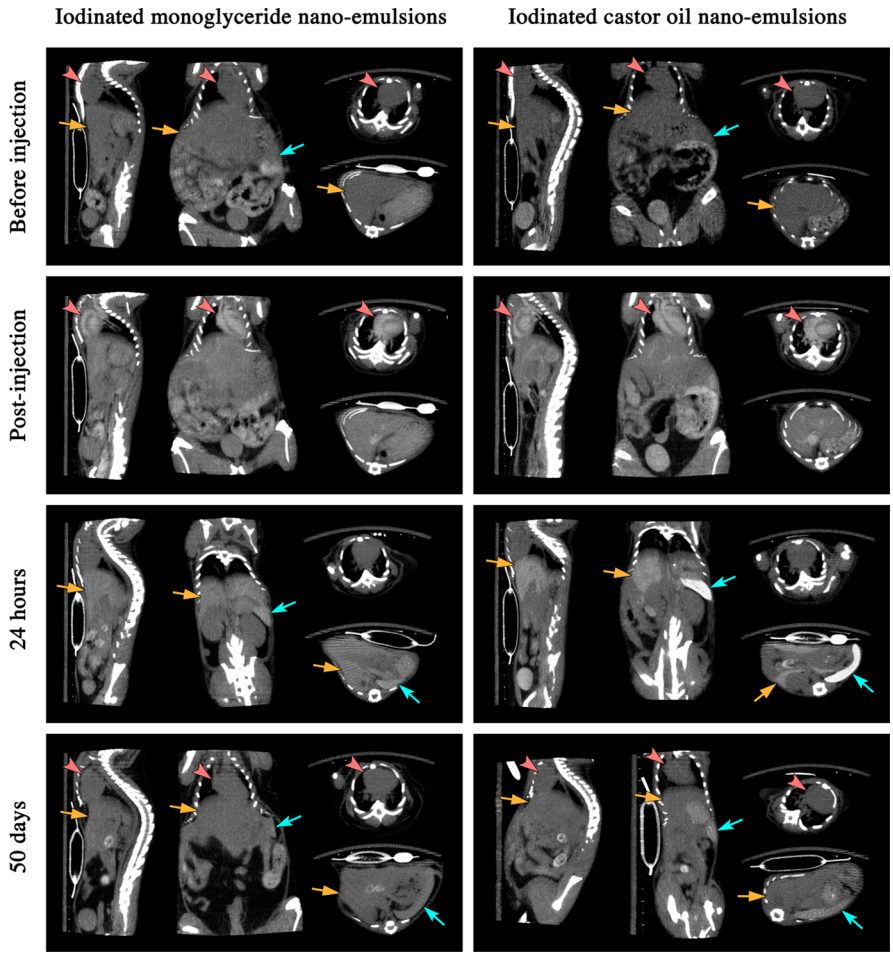

Figure 5. ***In vivo*** **micro-CT imaging (maximum projection intensity) of iodinated monoglycerides (left column) and iodinated castor oil (right column) nano-emulsions, at different representative times after i.v. injection. Each picture shows sagittal and coronal sections of the mice, as well as transverse slices through the heart, lung, and vertebra and transverse slices through the liver and spleen. Heart is indicated by red arrowheads, liver by orange arrows, and spleen by blue arrows.**

Three-dimensional volume rendering of liver and spleen induced by iodinated castor oil nano-emulsions 24 h after injection is given in Figure 6b. The strong contrast enhancement in spleen results in a very clear image that provides distinct details of the organ surface. In contrast, the liver appears less clearly, suggesting that the contrast agent is not homogeneously distributed and less concentrated than in the spleen. However, since the liver "compartment" dilutes more the contrast agent than the spleen, due to its much larger volume, it results in a difference in contrast enhancement that may not reflect the real amounts of contrast agent accumulated in the organs. This point was explored below with the quantification of the contrast agent in the different organs, by expressing the percent of injected dose as a function of the acquisition time. This approach shows that, though the contrast is higher in spleen than in liver, the total amount of contrast agent is higher in the liver. Since 3D image reconstructions were easily obtained due to the pronounced contrast induced by these iodinated systems, the latter appear thus as potent contrast agents for global structural imaging in micro-CT.

Quantification of contrast enhancement was followed up in blood (ROI in heart), liver, spleen, and kidneys over the 50 days of acquisition. Contrast enhancement is expressed as $\Delta HU(t)$, which is equal to the value of X-ray attenuation (normalized in Hounsfield units, HU) at acquisition time t subtracted by the one of the same region, before contrast agent administration. Pharmacokinetics and biodistribution in each organ of the two iodinated nano-emulsions are reported in Figure 7, in comparison with a previously described nano-emulsion of iodinated vitamin E (α-tocopherol).[5] Interestingly, these three formulations are identical in their surfactant and bulk composition and only differ by the nature of their oily core.

The contrast enhancement and kinetics in the blood pool appeared very similar for the three formulations. This can be easily understood considering that blood clearance is mediated by mechanisms involving recognition of particles through their surface properties. Since all iodinated nano-emulsions tested have the

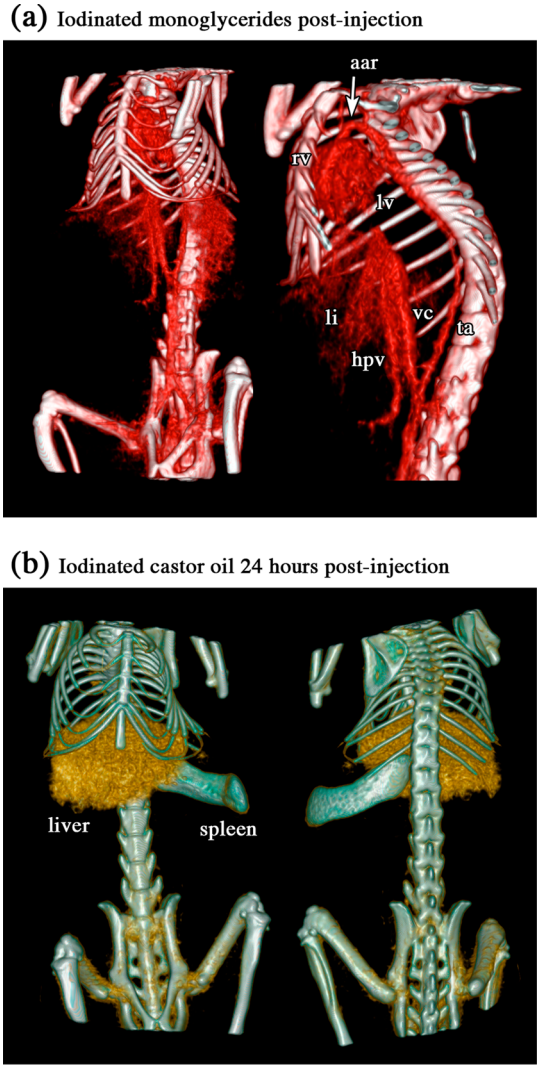

Figure 6. *In vivo* **micro-CT 3D volume rendering, (a) 5 min after injection of iodinated monoglycerides and (b) 24 h after injection of iodinated castor oil. Annotations: (aar) aortic arch, (rv) right ventricle, (lv) left ventricle, (li) location of liver, (vc) vena cava, (hpv) hepatic portal vein, (ta) thoracic aorta. Two movies corresponding to these volume rendering (a) and (b) are available as Supporting Information (movie1.mov and movie2.mov).**

same surface composition, this readily explains their very close blood clearance kinetics, giving half-life values of 6.1, 6.7, and 9.0 h for iodinated monoglyceride, castor oil, and vitamin E nano-emulsions, respectively. All three contrast agents can thus be used as blood pool contrast agents and have actually longer circulation half-lives than the majority of contrast agents reported in the literature. It is, however, worth noting that some liposomal iodinated formulations[7] can reach iodine concentrations as high as 150 mg/mL of iodine with half-lives around 24 h. Here, after 24 h, the value of ΔHU in the blood was observed to go back to zero. The performances of iodinated nano-emulsions can be further compared with those of other commercially available contrast agents such as, for instance, gold-based nanoparticles (AuroVist)[27] and rare earth-based nanoparticles (ExiTron nano 12000)[28] on the same animal model. In the present study, we obtained an initial contrast enhancement ΔHU = 200−240 HU that corresponds to an increase of the contrast of 300−330%, which is significantly higher than the 260 and 170% values reported in the literature[27] for AuroVist 15 nm and ExiTron Nano 12000, respectively. To allow the comparison of the data of Figure 7 (expressed in ΔHU) with values expressed in percentage of contrast enhancement (as both can be found in literature), we reported in Figure S2 (Supporting Information) that the pharmacokinetics data expressed in percentage of contrast enhancement with the reference before injection can be fixed at 100%. On the other hand, the half-life around 6 or 9 h is optimal for CT scans and comparable or better than that reported for the two commercial contrast agents.

The ΔHU values of our iodinated nano-emulsions in the liver and the spleen increased progressively with time, reaching a maximum 24 h postinjection. To verify whether the potential aggregation of nanodroplets in blood circulation could explain the differences in these pharmacokinetics, the size of nano-emulsions incubated in fetal bovine serum (FBS) for different times and at different dilutions was studied by DLS. The results reported in Figure S3 (Supporting Information) show almost invariant size for all experimental conditions, thus confirming the high stability of these iodinated nano-emulsions in FBS. After this maximum, the ΔHU values slowly decreased. Finally, the highest ΔHU values in the kidneys were observed within the first hour and then progressively decreased with time. Thus, these data suggest that the nanodroplets gradually eliminated from the blood circulation accumulate mainly in liver and spleen. After 24 h, once nano-emulsions are cleared from the bloodstream, the contrast enhancement also starts decreasing in liver and spleen, indicating that they are progressively eliminated from these organs.

In contrast to vitamin E nano-emulsions for which the elimination is governed by hepatocyte-selective uptake,[5] the accumulation of the iodinated monoglyceride and castor oil nano-emulsions in the spleen suggests an elimination by the reticulo-endothelial system.[5] Interestingly, iodinated castor oil nano-emulsions show an outstanding contrast for the spleen, with a maximum ΔHU value of 530 ± 50 HU. The maximum ΔHU values obtained with iodinated monoglyceride nano-emulsions for the same organ were somewhat lower, being 220 ± 30 HU. In comparison, much lower contrast was seen in the liver with these two formulations since their maximum ΔHU values were 130 ± 15 and 76 ± 6 HU, respectively.

To get further information on their pharmacokinetics, the elimination and accumulation kinetics of all three iodinated formulations were fitted with classical monocompartmental exponential eqs 1 and 2,

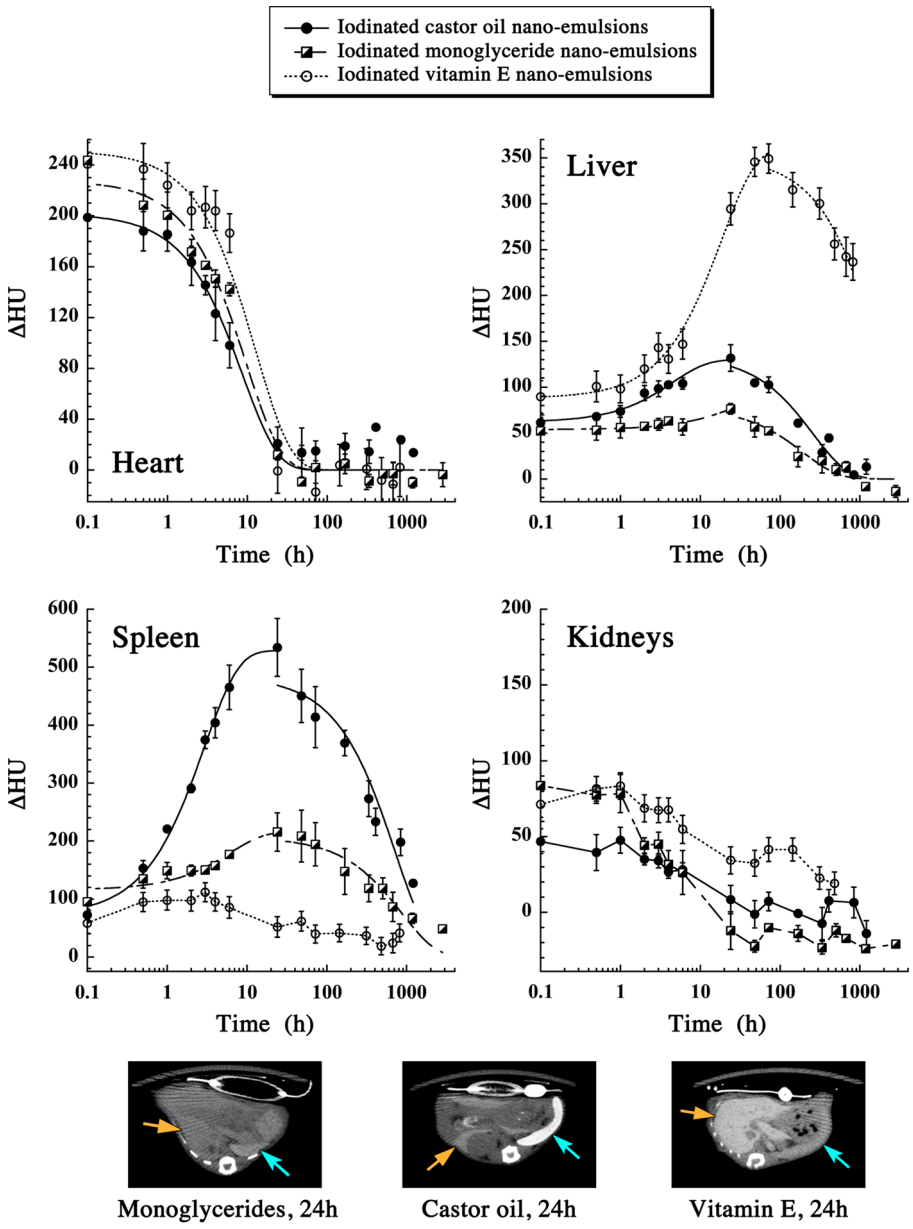

Figure 7. Dependence of the X-ray attenuation with time after i.v. administration of iodinated nano-emulsions. Iodinated monoglycerides and iodinated castor oil nano-emulsions are compared to each other in heart, liver, spleen, and kidneys and also compared with iodinated vitamin E (α-tocopherol) nano-emulsions from literature (data for iodinated vitamin E reproduced with permission from ref 5; copyright 2013 Elsevier); n = 3 for each nano-emulsion. Curves were fitted with eq 1 for the heart and eqs 2 and 3 for the liver and spleen (eq 2 for accumulation and eq 3 for elimination). To illustrate the differences in contrast at 24 h postinjection, transverse slices through the liver and spleen are presented. Liver is indicated by orange arrows and spleen by blue arrows.

respectively:

$$\Delta HU(t) = \Delta HU_0 \times \exp(-k_1 t) \quad (1)$$

$$\Delta HU(t) = \Delta HU_0 + \Delta HU_\infty \times (1 - \exp(-k_2 t)) \quad (2)$$

where ΔHU_0 is the initial value of the contrast enhancement in blood (after injection), ΔHU_∞ is the contrast enhancement at the end of the accumulation process (*i.e.*, increment above the ΔHU_0 value), k_1 is the blood elimination rate constant, and k_2 is the accumulation rate constant. Afterward, once blood clearance is over at 24 h, the clearance from liver and spleen becomes visible, following a monoexponential decrease given by eq 3:

$$\Delta HU(t) = \Delta HU_0 \times \exp(-k_3(t - 24)) \quad (3)$$

where k_3 is the liver or spleen elimination rate. The values of the different parameters (Table 1) were obtained from the fits shown in Figure 7 for the elimination of the iodinated compounds from blood (k_1 and $t_{1/2}$), their accumulation in liver and spleen (k_2), and their elimination from liver and spleen (k_3 and $t_{1/2}$). For the blood clearance, the values of the elimination rate k_1 are comparable for the three formulations,

TABLE 1. Pharmacokinetics Parameters for the Iodinated Nano-Emulsions[a]

	iodinated castor oil			iodinated monoglyceride			iodinated vitamin E		
	blood	liver	spleen	blood	liver	spleen	blood	liver	spleen
ΔHU_0 (HU)	202	62	72	228	54	116	245	88	58
k_1 (h^{-1})	0.113			0.103			0.077		
$t_{1/2}$ (h)	6.1			6.7			9.0		
k_2 (h^{-1})		0.224	0.345		0.037	0.164		0.054	
ΔHU_{max} (HU)		132	534		76	216		349	111
k_3 (h^{-1})		0.0039	0.0014		0.0051	0.0012		0.00054	
$t_{1/2}$ (days)		7.4	21.1		5.6	24.9		53	

[a] $\Delta HU_{max} = \Delta HU_0 + \Delta HU_\infty$.

being only slightly higher for the iodinated castor oil and monoglycerides (0.113 and 0.103 h^{-1}) than for vitamin E (0.077 h^{-1}). This difference is probably due to the major role of the spleen in the clearance process for the iodinated castor oils and monoglycerides nanoemulsions. Indeed, the values of the accumulation rate k_2 (0.345 and 0.164 h^{-1}, for the iodinated castor oil and monoglyceride, respectively) in the spleen are at least 3-fold higher than the corresponding rate in the liver for vitamin E (0.054 h^{-1}) for which the role of spleen is negligible. It is also interesting to note that the kinetics of accumulation in liver and spleen are comparable for iodinated castor oil (k_2^{liver} = 0.224 h^{-1} and k_2^{spleen} = 0.345 h^{-1}) but not for monoglycerides (k_2^{liver} = 0.037 h^{-1} and k_2^{spleen} = 0.164 h^{-1}).

Once the blood is cleared from the contrast agent, the metabolism and elimination of iodinated oils from the liver or spleen remain the only observable kinetics. These elimination kinetics are much slower than the accumulation kinetics ($k_3 \ll k_2$, Table 1). Globally, the iodinated castor oil and monoglycerides present similar elimination kinetics, with half-lifetimes of about 1 week in the liver and 3 weeks in the spleen. It follows that these contrast agents are largely removed from the body within 50 days. Finally, contrast enhancement in kidneys begins in the range of 50 to 90 HU and decreases along with the blood clearance. This signal likely corresponds to the renal filtration of a part of the nanodroplets, that is, the smaller population of the log-normal distribution, but can also be induced by elimination of metabolites after their passage in liver or spleen.

The raw contrast enhancement given by the value of ΔHU is fundamental for imaging applications but does not give a direct idea of the biodistribution of the contrast agent in organs or biological compartments since their volumes are different. To determine the real biodistribution of the contrast agents, we expressed the percentages of injected dose for each compartment or organ of interest: blood pool, liver, and spleen. Taking into account that the liver of a Swiss mouse represents 4.37 ± 0.19% of its body weight and the spleen represents 0.48 ± 0.13%,[29] we recalculated

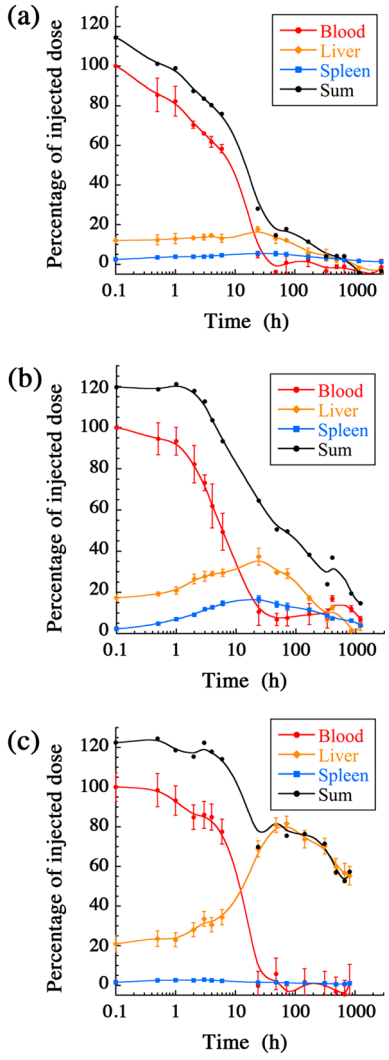

Figure 8. Accumulation and elimination of iodinated monoglycerides (a), castor oil (b), and vitamin E (c) in different organs. The contrast agents were expressed as the percentage of injected dose, using the images from Figure 7 and placing the ROIs in the blood pool (red), liver (orange), and spleen (blue). The summed percentages (black) are also shown.

the amount of contrast agent (as % of injected dose) in the different organs at different acquisition times (Figure 8). Using this representation, monoglycerides

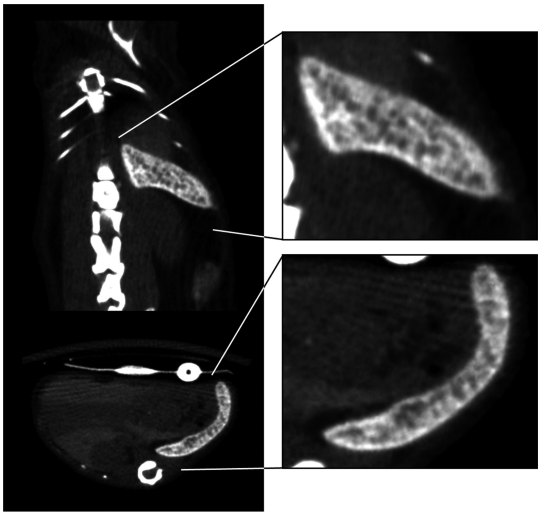

Figure 9. Micro-CT imaging and maximum intensity projections. Magnified representations of the spleen, 24 h after injection of iodinated castor oil: sagittal (top left), coronal (top right), and transverse (bottom) section.

(Figure 8a) show a moderate accumulation in liver (around 17% at the maximum, 24 h) and negligible accumulation in spleen (~5% at 24 h). In contrast, castor oil (Figure 8b) accumulates much stronger in the liver (40% at 24 h) but less in the spleen (20% at 24 h). Its global elimination kinetics is close to that of monoglycerides, with a gradual clearance after 24 h (compare black curves in Figure 8a,b). In the case of vitamin E (Figure 8c), the accumulation is much higher in the liver (reaching 80% of the injected dose at 48 h) with nearly nothing in the spleen. Its elimination kinetics is also quite different, showing a longer retention time in the liver. Thus, a different mechanism may be involved in the accumulation and elimination of vitamin E as compared to monoglycerides and castor oil. Noticeably, the initial presence of the contrast agent in liver comes from the blood irrigating the liver that contains contrast agents, explaining the apparent sum values (overall blood + liver) higher than 100%.

The main results from these data are (i) the similar kinetics of the blood clearance that is likely due to the similar surface composition of the nano-emulsion droplets, inducing a similar behavior from the blood clearance system; and (ii) the clear differences in their elimination pathway. Spleen accumulation could be linked to recognition by immune cells. In Figure 9, which focuses on the spleen at the maximum contrast enhancement (24 h after injection of iodinated castor oil nano-emulsion), one can observe a heterogeneity in the distribution of the contrast agent within the spleen.

The less contrasted domains correspond to the white pulp, consisting of lymphoid tissues mainly composed of leucocytes from different lineages, such as lymphocytes. In contrast, the more contrasted part corresponds to the red pulp in which the blood is filtered and which is composed of venous cavities filled with red blood cells, lymphocytes, and macrophages.[30] Therefore, the accumulation of the contrast agent in the spleen is likely linked to the differential recognition of the oil droplets or leaked oil by immune cells as a function of their chemical structure. The slight shift in the size distribution between both formulations (see Figure 2) could also have been invoked to explain the differences in the accumulation behaviors since the smaller particles may be more excreted by kidneys while the larger ones may be trapped by the spleen. However, the difference in the values of the contrast is so high (ΔHU_{max} values are 220 ± 30 and 530 ± 30 HU) that it can only be explained by alternative reasons, such as differences in the affinities of the droplets or their content for the spleen tissues or enhanced recognition by immune cells, especially macrophages. Interestingly, vitamin E nano-emulsions are not accumulated in spleen but in liver through specific hepatocyte uptake. The marginal accumulation of iodinated vitamin E nanodroplets in the spleen may result from their low ability in comparison to iodinated monoglycerides and castor oil to be taken up by macrophages. To confirm this hypothesis, iodinated nano-emulsion droplets were loaded with a lipophilic dye (NR668) and incubated with mouse macrophages to follow their uptake. NR668 is a Nile Red derivative bearing aliphatic chains, ensuring the dye remains encapsulated within the nano-emulsion lipid droplets, even in the presence of a serum-containing medium or when injected in a zebrafish model.[31] Nanodroplets with different iodinated oils, formulated together with 1 wt % of NR668, showed fluorescence maxima centered in the range of 590−605 nm, indicating that the dye was successfully encapsulated inside the apolar core.[31] Iodinated monoglyceride and castor oil nano-emulsion droplets were observed to be gradually taken up by the macrophages (Figure 10). After 30 min incubation, macrophages only engulfed a few droplets near the plasma membrane. Their number significantly increased after 2 h incubation, gradually highlighting the whole cell periphery (see image with only red channel of NR668). Finally, after 1 day of incubation, the whole cytoplasm is filled with nano-emulsion droplets. In sharp contrast, the fluorescence of NR668 was not detectable in macrophages incubated with iodinated vitamin E nano-emulsions, validating our hypothesis that this poor uptake may be responsible for the low accumulation of iodinated vitamin E droplets in the spleen. To check whether this difference in the nanodroplet uptake between monoglyceride, castor oil, and vitamin E is specific to the macrophage cell type, we compared by fluorescent microscopy the uptake of NR668-loaded nano-emulsion droplets (made with the three different iodinated oils) by murine hepatocytes BNL-CL2 and macrophages RAW264.7, after 30 min and 24 h incubation (Figure S4, Supporting Information). In hepatocytes, no internalization of nano-emulsion droplets

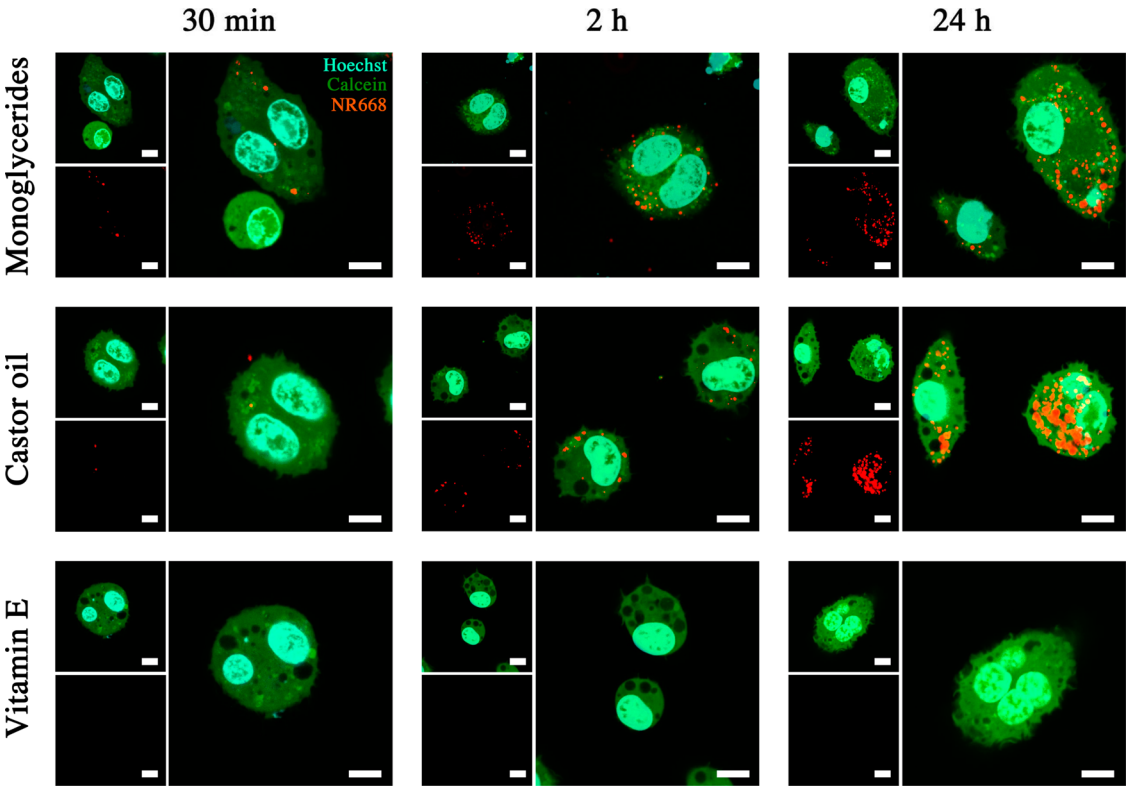

Figure 10. Monitoring of the uptake of NR668-loaded iodinated nano-emulsions by murine macrophages (RAW264.7 cells). Nuclei were stained with Hoechst (cyan) and cells with calcein AM (green). NR668 (a lipophilic modified Nile Red) loaded in the oil core of the nano-emulsion droplets allows following the location of the droplets once engulfed by the cells. Iodinated monoglycerides, iodinated castor oil, and iodinated vitamin E were formulated as nano-emulsions and incubated for different times: 30 min, 2 h, and 24 h. Top left insets show the cell and nuclei. Bottom left insets show the signal of NR668, and the larger right picture shows both merged.

was observed with all three iodinated oils, confirming that the uptake by macrophages of nano-emulsions made from castor oil and monoglycerides (Figure 10) is selective.

These data clearly show that the oil nature has a strong impact on macrophage uptake, even formulated as nanodroplets with similar surface composition. They allow understanding of the selective accumulation in the spleen of iodinated monoglycerides and castor oil. To confirm our microscopy observations, a quantification of the internalized NR668 was performed by fluorometry of the cellular lysate in DMSO (Figure 11).

These data confirmed the uptake of nanodroplets containing monoglycerides and castor oil. The measured values appear similar for the two oils, with some difference arising only after 24 h, a condition that is relatively far from the conditions used *in vivo*. Importantly, even at such long incubation time, the vitamin E nanodroplets do not penetrate into cell cytoplasm. This confirms that vitamin E droplets and/or the vitamin E oil are not recognized by macrophages, and that the blood clearance in this case occurs through the gradual accumulation of the droplets in hepatocytes. This difference in the clearance mechanism can also explain the longer half-life (9.0 h) of vitamin E

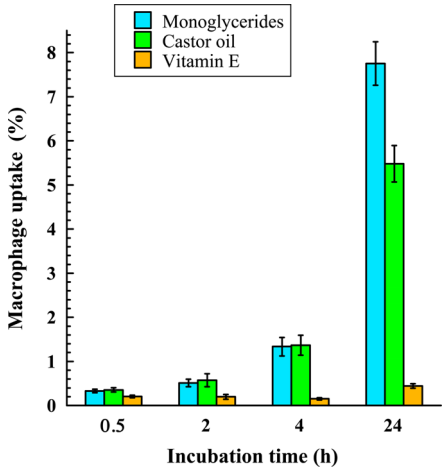

Figure 11. Quantification of nano-emulsion uptake by macrophages as a function of incubation time and oil nature. After incubation with NR668-loaded nanodroplets, the macrophages were washed, lysed with DMSO, and measured by fluorometry. Uptake was expressed as the percentage of fluorescence associated with cells *versus* the amount of fluorescence present in the feed solution.

nano-emulsions compared to castor oil (6.1 h) and monoglycerides (6.7 h). The results of macrophage uptake explains the difference in accumulation in liver and spleen between vitamin E and the two other oils

but does not permit one to conclude on the difference of accumulation between iodinated monoglycerides and iodinated castor oil, likely due to additional factors arising *in vivo*, as compared to *in vitro* cell experiments.

CONCLUSION

This study shows that iodinated nano-emulsions with comparable morphologies, sizes, surface composition, and only differing in the chemical nature of the iodinated oil droplet core display significantly different pharmacokinetics and biodistributions. Herein we propose two novel formulations based on hexa-iodinated monoglyceride and hexa-iodinated castor oil, formulated by spontaneous emulsification and stabilized by PEGylated non-ionic surfactant. Besides the very high contrasting properties of these X-ray contrast agents, we show that, after i.v. administration, both nano-emulsions present similar blood elimination kinetics with $t_{1/2}$ around 6 h, followed then by different *in vivo* behavior, with the iodinated castor oil showing a much stronger accumulation in the spleen. Comparison with another iodinated nano-emulsion based on iodinated vitamin E that accumulates only in liver further demonstrates that these nanoparticulate systems can provide strong X-ray contrast enhancement in specific targets such as liver, spleen, or only blood as a function of the oil used in the nano-emulsion formulation. Our data further revealed that the nature of the iodinated oil affects the uptake of nanodroplets by the macrophages, thus explaining in part the observed differences in biodistribution. The half-elimination time of these contrast agents is on the scale of weeks, offering sufficient retention for micro-CT imaging applications. Their potential use for clinical imaging could be envisioned, as well.

EXPERIMENTAL SECTION

2,3,5-Triiodobenzoic acid, castor oil, *N*,*N*′-dicyclohexylcarbodiimide, 4-dimethylaminopyridine, deuterated chloroform ($CDCl_3$), ethyl acetate, cyclohexane, dichloromethane, sodium bicarbonate, sodium sulfate anhydrous, sodium chloride Hoechst 33258, calcein AM, dimethyl sulfoxide (DMSO), and 3-(4,5-dimethylthiazol-2-yl)-2,5-diphenyltetrazolium bromide (MTT) solutions were purchased from Sigma-Aldrich (St. Louis, MO). Glyceryl monocaprylate (Capmul MCM C8) was kindly gifted by Abitec (Columbus, OH). Non-ionic surfactant (Kolliphor ELP) from BASF (Ludwigshafen, Germany) was kindly donated by Laserson, Etampes, France. Kolliphor ELP (formerly named "Cremophor ELP") is a parenteral-grade non-ionic surfactant made by reacting ethylene oxide to castor seed oil at a molar ratio of 35.[32] Phosphate buffered saline, Dulbecco's modified Eagle medium (DMEM), and fetal bovine serum were from PAN Biotech (Aidenbach, Germany).

General Synthesis of Hexa-iodinated Monoglyceride and Hexa-iodinated Castor Oil. 2,3,5-Triiodobenzoic acid (TIBA) (10 g, 0.02 mol), 4-dimethylaminopyridine (0.75 g, 0.007 mol), and *N*,*N*′-dicyclohexylcarbodiimide (4.5 g, 0.022 mol) were sequentially added to a solution containing either glyceryl monocaprylate (1.84 g, 0.0085 mol) or castor oil (7.92 g, 0.0085 mol), in dichloromethane at room temperature. The reaction mixture was stirred overnight at room temperature. Then, dicyclohexylurea and other precipitates were removed by filtration. The organic phase was washed twice with saturated aqueous $NaHCO_3$ and once with saturated NaCl solution and then dried over anhydrous Na_2SO_4. The solvent was removed by rotary evaporator, and the resulting oil was purified by gradient elution silica gel column chromatography using cyclohexane and ethyl acetate as eluents. Both purified products were obtained as dense and yellowish viscous oils. The reaction yields were 58% for hexa-iodinated monoglyceride and 47% for hexa-iodinated castor oil. The chemical structure of these two iodinated oils is presented in Figure 1a. Hexa-iodinated monoglyceride and hexa-iodinated castor oil have theoretical iodine content of 64.5 and 40.2 wt %, respectively. It should be noted that the difference in molecular weights between these two molecules can also play a role in their X-ray attenuation properties, which are the highest for the heaviest one (*i.e.*, iodinated castor oil).

Characterization of Hexa-iodinated Monoglyceride and Hexa-iodinated Castor Oil. ^{1}H NMR spectra were recorded with a Bruker Top Spin 3.0 operating at 400 MHz using deuterated chloroform ($CDCl_3$) as a solvent. Chemical shifts (δ) were expressed in parts per million, taking tetramethylsilane as internal reference. *Hexa-iodinated monoglycerides:* ^{1}H NMR ($CDCl_3$, δ/ppm) 8.2 (s, 2H, ortho), 7.7 (s, 2H, para), 4.6 (d, 2H, phCOO−CH_2−CH), 4.4 (m, 1H, CH_2−CH−CH_2), 4.3 (d, 2H, OCH_2−CH), 2.3 (t, 2H, CO−CH_2−CH_2), 1.5 (m, 2H, $COCH_2$−CH_2−CH_2), 1.3 (m, 8H, CH_2−CH_2)$_4$−CH_3), 0.8 (t, 3H, CH_3). *Hexa-iodinated castor oil*: ^{1}H NMR ($CDCl_3$, δ/ppm) 8.2 (s, 2H, ortho), 7.6 (s, 2H, para), 5.5 (dd, 6H, (CH=CH)$_3$), 5 (m, 1H, OCH_2−CH−CH_2), 4.2 (d, 4H, (COO−CH_2−CH)$_2$), 3.5(m, 3H, CH_2−CH−OCOPh), 2.4 (t, 6H, (OCO−CH_2−CH_2)$_3$), 2.2 (t, 6H, (CH−CH_2−CH=CH)$_3$), 2.1 (m, 6H, (CH_2−CH_2−CH=CH)$_3$), 2 (s, 1H, OH), 1.5 (m, 6H, ($COCH_2$−CH_2−CH_2)$_3$), 1.3 (q, 6H, (PhCOO−CH−CH_2)$_3$), 1.2 (m, 48H, (CH−(CH_2)$_4$−CH_3)$_3$, (CH=CHCH_2-(CH_2)$_4$−CH_2)$_3$), 0.8 (t, 9H, (CH_3)$_3$).

Preparation of Iodinated Nano-Emulsions. Nano-emulsions of iodinated monoglyceride and iodinated castor oil were formulated by the spontaneous nano-emulsification method as previously reported.[26,33−35] Formulation parameters are defined as surfactant/(surfactant + oil) weight ratio (SOR) and (surfactant + oil)/(surfactant + oil + water) weight ratio (SOWR).[26] (i) Iodinated monoglyceride nano-emulsions are formulated with SOR = 60% and SOWR = 40%. Hexa-iodinated monoglyceride (0.32 g) was first mixed with the non-ionic hydrophilic surfactant (0.48 g), maintained at 70 °C, and homogenized by help of several vortex mixing and use of a sonication bath (around 10 min). Next, PBS, used as an aqueous phase (1.20 g), was added to the surfactant/oil mixture under gentle magnetic stirring, giving rise within seconds to spontaneous formation of stable nano-emulsions. A nano-emulsion droplet is schematically represented in Figure 1b. (ii) Iodinated castor oil nano-emulsions are formulated at SOR = 65% and SOWR = 40%. The formulation process, similar to the one described above, uses hexa-iodinated castor oil (0.28 g), non-ionic surfactant (0.52 g), and PBS (1.2 g). The SOR values used for both formulations were selected to obtain nano-emulsions with optimal nano-emulsion size, monodispersity, and iodine content, as described in the Results and Discussion section (Figure 2).

Characterization of Nano-Emulsions. *Dynamic Light Scattering.* Size distributions and polydispersity indices (PDI) were measured by DLS with a NanoZS Malvern apparatus (Malvern, Orsay, France). The helium/neon laser, 4 mW, was operated at 633 nm, with the scatter angle fixed at 173° and the temperature maintained at 25 °C. DLS data were analyzed using a cumulant-based method.

Transmission Electron Microscopy. The X-ray attenuation properties of iodine nanodroplets also result in good contrast in TEM. Therefore, samples were used without any staining agent and were diluted (1/10) with Milli-Q water. A drop of the suspension was placed on a carbon grid (carbon type-A, 300 mesh, copper, Ted Pella Inc. Redding, PA) and dried at 40 °C.

Observations were carried out using a Philips Morgagni 268D electron microscope.

Cytotoxicity Assays. Cytotoxicity assays were performed using HeLa human cervix epithelial adenocarcinoma cells, BNL-CL2 mouse hepatocyte, and RAW264.7 murine leukemia virus-transformed monocyte cells. HeLa cells were selected because they are considered to be a standard cell line that allows direct comparison of experimental data. RAW264.7 cells were chosen because their properties are very similar to those of normal macrophages.[36] RAW264.7 cells are a well-suited model for macrophages,[37−39] showing notably similar patterns of uptake and cytotoxicity as primary macrophages.[39] Cells were seeded in 96-well plates at a concentration of 10^4 cells per well in 100 μL of medium (DMEM) containing 10% FBS and 1 wt % of commercial solution of penicillin and streptomycin. Cells were then incubated overnight at 37 °C under a controlled atmosphere (5% CO_2 and 80% H_2O). Next, the culture medium was replaced by the same medium but containing variable concentrations of iodine encapsulated nano-emulsions (see details below). After incubation for 24 h, the medium was removed and the cells were washed with PBS. Then, the wells were filled with cell culture medium containing MTT, incubated for 4 h at 37 °C, and the formazan crystals formed were dissolved by adding 100 μL of DMSO. UV absorbance was measured at 570 nm with a microplate reader (Varioskan Flash, Thermo Scientific, USA). Experiments were carried out in triplicate and expressed as a percentage of viable cells compared to the control group.

***In Vitro* Mouse Macrophage Uptake.** *Confocal Microscopy.* The cellular uptake and intracellular localization were determined in RAW264.7 cells (mouse macrophages) using a Leica TCS SP confocal scanning system (Leica, Germany). To follow the nano-emulsion droplets, we used a modified lipophilic Nile Red (NR668) that was solubilized at 0.1% (wt/wt) in the iodinated oils before formulation of nano-emulsions. NR668 synthesis was previously reported.[31] Cells were cultured overnight in cell culture glass chambers slides at a density of 5×10^4 cells per well before their exposition to the dye-loaded nano-emulsions in DMEM at a concentration corresponding to 0.1 mg/mL, supplemented with 10% of FBS, for 30 min, 2 h, and 24 h at 37 °C in a 5% CO_2 humidified atmosphere. After incubation, cells were stained with calcein AM (10 μM, 15 min of incubation in HBSS) and with Hoechst 33342 (50 μM, 10 min of incubation in HBSS). After six washes in HBBS to remove all nonpenetrated nano-emulsion droplets, cells were mounted in the fluorophore protector CC/mount and observed with a Leica confocal microscope equipped with an argon/neon laser and a 63× oil immersion objective. The excitation wavelengths used were 360 nm for Hoechst 33342, 488 nm for calcein, and 543 nm for NR668, and the fluorescence signals were collected in the 380−460 nm range for Hoechst, 500−530 nm range for calcein, and 560−650 nm range for Nile Red 668, respectively. The images were processed with Fiji software.

Quantification of Macrophage Uptake. Cellular uptake was quantified by fluorescence spectroscopy. Mouse macrophage RAW264.7 cells were cultured as described in the paragraph above, except that cells were lysed with DMSO and not mounted for microscopy analysis. The effectiveness of washing and lysing was checked with fluorescence microscopy observations. The concentration of encapsulated NR668 in the cell lysate was quantified by fluorimetry with an excitation wavelength of 550 nm and an emission wavelength of 630 nm (with a microplate reader Varioskan Flash, Thermo Scientific, USA). Uptake was expressed as the percentage of fluorescence associated with cells *versus* the amount of fluorescence in the feed solution.

Micro-CT Imaging. The experiments were performed in agreement with the Committee of Animal Research and Ethics of the University of Lyon-1.

In Vitro Experiments. The X-ray attenuation properties of iodinated nano-emulsions were evaluated at various concentrations with a micro-CT scanner (1076 Skyscan, Kartuizersweg, Belgium). Experimental parameters were as follows: X-ray, 49 keV, 129 μA; resolution, 35 mm; pitch, 0.4°; aluminum filters, 0.5 and 632 ms. Iodine concentration of nano-emulsions was determined using a calibration curve established with a commercial hydrophilic contrast agent (XenetiX 300, *i.e.*, iobitridol), correlating iodine concentration and radiopacity.

In Vivo Experiments. In vivo imaging experiments were performed with a micro-CT scanner (INVEON, Siemens, Munich, Germany). The experimental X-ray parameters were as follows: X-ray, 50 keV, 500 μA; resolution, 111.25 μm; pitch, 2°; aluminum filters, 0.5 and 900 ms. The acquisitions were performed on Swiss mice, n = 3, for each type of nano-emulsion. Before acquisition, mice were anesthetized with isoflurane. Then, iodinated nano-emulsions were intravenously injected (using a catheter) in the tail vein, with an injection volume corresponding to 10% of the blood volume (*i.e.*, 7.6 μL of nano-emulsions per gram of mouse). Scans were performed before administration, immediately after injection, and after 30 min, 1 h, 2 h, 3 h, 4 h, 6 h, 1 day, 2 days, 3 days, 7 days, 14 days, 21 days, 28 days, and 50 days. The micro-CT raw data were treated with OsiriX viewer to establish 2D maximum projection slices and 3D volume rendering images and then to quantify the signal by placing the region of interests in the heart, liver, spleen, and kidneys.

Conflict of Interest: The authors declare no competing financial interest.

Acknowledgment. Experimental part (*in vivo* imaging) of this study was performed on CERMEP-imagerie du vivant, Bron, F-69677, France, imaging facilities. The authors thank the technical staff of the platform. M.C. would like to acknowledge Grant "Attractivité IDEX 2013" within the University of Strasbourg, France.

Supporting Information Available: Additional figures and movies as described in the text. This material is available free of charge *via* the Internet at http://pubs.acs.org.

REFERENCES AND NOTES

1. Li, X.; Anton, N.; Zuber, G.; Vandamme, T. F. Contrast Agents for Preclinical Targeted X-ray Imaging. *Adv. Drug Delivery Rev.* **2014**, *76*, 116–133.
2. Anton, N.; Vandamme, T. F. Nanotechnology for Computed Tomography: A Real Potential Recently Disclosed. *Pharm. Res.* **2014**, *31*, 20–34.
3. Hallouard, F.; Anton, N.; Choquet, P.; Constantinesco, A.; Vandamme, T. F. Iodinated Blood Pool Contrast Media for Preclinical X-ray Imaging Applications: A Review. *Biomaterials* **2010**, *31*, 6249–6268.
4. Jakhmola, A.; Anton, N.; Vandamme, T. F. Inorganic Nanoparticles Based Contrast Agents for X-ray Computed Tomography. *Adv. Healthcare Mater.* **2012**, *1*, 413–431.
5. Li, X.; Anton, N.; Zuber, G.; Zhao, M.; Messaddeq, N.; Hallouard, F.; Fessi, H.; Vandamme, T. F. Iodinated Alpha-Tocopherol Nano-Emulsions as Non-toxic Contrast Agent for Preclinical X-ray Imaging. *Biomaterials* **2013**, *34*, 481–491.
6. van Tellingen, O.; Beijnen, J.; Verweij, J.; Scherrenburg, E.; Nooijen, W.; Sparreboom, A. Rapid Esterase-Sensitive Breakdown of Polysorbate 80 and Its Impact on the Plasma Pharmacokinetics of Docetaxel and Metabolites in Mice. *Clin. Cancer Res.* **1999**, *5*, 2918–2924.
7. Badea, C. T.; Athreya, K. K.; Espinosa, G.; Clark, D.; Ghafoori, A.; Li, Y.; Kirsch, D. G.; Johnson, G.; Annapragada, A.; Ghaghada, K. B. Computed Tomography Imaging of Primary Lung Cancer in Mice Using a Liposomal-Iodinated Contrast Agent. *PLoS One* **2012**, *7*, e34496.
8. Toy, R.; Hayden, E.; Camann, A.; Berman, Z.; Vicente, P.; Tran, E.; Meyers, J.; Pansky, J.; Peiris, P. M.; Wu, H.; Exner, A.; Wilson, D.; Ghaghada, K. B.; Karathanasis, E. Multimodal *In Vivo* Imaging Exposes the Voyage of Nanoparticles in Tumor Microcirculation. *ACS Nano* **2013**, *7*, 3118–3129.
9. de Vries, A.; Custers, E.; Lub, J.; van den Bosch, S.; Nicolay, K.; Grull, H. Block-Copolymer-Stabilized Iodinated Emulsions for Use as CT Contrast Agents. *Biomaterials* **2010**, *31*, 6537–6544.
10. Wisner, E. R.; Weichert, J. P.; Longino, M. A.; Counsell, R. E.; Weisbrode, S. E. A Surface-Modified Chylomicron

Remnant-like Emulsion for Percutaneous Computed Tomography Lymphography: Synthesis and Preliminary Imaging Findings. *Invest. Radiol.* **2002**, *37*, 232–239.
11. Pan, D.; Williams, T. A.; Senpan, A.; Allen, J. S.; Scott, M. J.; Gaffney, P. J.; Wickline, S. A.; Lanza, G. M. Detecting Vascular Biosignatures with a Colloidal, Radio-opaque Polymeric Nanoparticle. *J. Am. Chem. Soc.* **2009**, *131*, 15522–15527.
12. Jakhmola, A.; Anton, N.; Anton, H.; Messaddeq, N.; Hallouard, F.; Klymchenko, A.; Mely, Y.; Vandamme, T. F. Poly-ε-Caprolactone Tungsten Oxide Nanoparticles as a Contrast Agent for X-ray Computed Tomography. *Biomaterials* **2014**, *35*, 2981–2986.
13. Brigger, I.; Dubernet, C.; Couvreur, P. Nanoparticles in Cancer Therapy and Diagnosis. *Adv. Drug Delivery Rev.* **2002**, *54*, 631–651.
14. Haley, B.; Frenkel, E. Nanoparticles for Drug Delivery in Cancer Treatment. *Urol. Oncol.* **2008**, *26*, 57–64.
15. Torchilin, V. P.; Trubetskoy, V. S. Which Polymers Can Make Nanoparticulate Drug Carriers Long-Circulating?. *Adv. Drug Delivery Rev.* **1995**, *16*, 141–155.
16. Betzer, O.; Shwartz, A.; Motiei, M.; Kazimirsky, G.; Gispan, I.; Damti, E.; Brodie, C.; Yadid, G.; Popovtzer, R. Nanoparticle-Based CT Imaging Technique for Longitudinal and Quantitative Stem Cell Tracking within the Brain: Application in Neuropsychiatric Disorders. *ACS Nano* **2014**, *8*, 9274–9285.
17. Cole, L. E.; Vargo-Gogola, T.; Roeder, R. K. Detection of Breast Microcalcifications in a Murine Model Using Targeted Gold Nanoparticles. *ACS Nano* **2014**, *8*, 7486–7496.
18. Kattumuri, V.; Katti, K.; Bhaskaran, S.; Boote, E. J.; Casteel, S. W.; Fent, G. M.; Robertson, D. J.; Chandrasekhar, M.; Kannan, R.; Katti, K. V. Gum Arabic as a Phytochemical Construct for the Stabilization of Gold Nanoparticles: *In Vivo* Pharmacokinetics and X-ray-Contrast-Imaging Studies. *Small* **2007**, *3*, 333–341.
19. Hainfeld, J. F.; Slatkin, D. N.; Focella, T. M.; Smilowitz, H. M. Gold Nanoparticles: A New X-ray Contrast Agent. *Br. J. Radiol.* **2006**, *79*, 248–253.
20. Kim, D.; Park, S.; Lee, J. H.; Jeong, Y. Y.; Jon, S. Antibiofouling Polymer-Coated Gold Nanoparticles as a Contrast Agent for *In Vivo* X-ray Computed Tomography Imaging. *J. Am. Chem. Soc.* **2007**, *129*, 7661–7665.
21. Eck, W.; Nicholson, A. I.; Zentgraf, H.; Semmler, W.; Bartling, S. Anti-Cd4-Targeted Gold Nanoparticles Induce Specific Contrast Enhancement of Peripheral Lymph Nodes in X-ray Computed Tomography of Live Mice. *Nano Lett.* **2010**, *10*, 2318–2322.
22. Chanda, N.; Kattumuri, V.; Shukla, R.; Zambre, A.; Katti, K.; Upendran, A.; Kulkarni, R. R.; Kan, P.; Fent, G. M.; Casteel, S. W.; Smith, C. J.; Boote, E.; Robertson, J. D.; Cutler, C.; Lever, J. R.; Katti, K. V.; Kannan, R. Bombesin Functionalized Gold Nanoparticles Show *In Vitro* and *In Vivo* Cancer Receptor Specificity. *Proc. Natl. Acad. Sci. U.S.A.* **2010**, *107*, 8760–8765.
23. Rabin, O.; Manuel Perez, J.; Grimm, J.; Wojtkiewicz, G.; Weissleder, R. An X-ray Computed Tomography Imaging Agent Based on Long-Circulating Bismuth Sulphide Nanoparticles. *Nat. Mater.* **2006**, *5*, 118–122.
24. Oh, M. H.; Lee, N.; Kim, H.; Park, S. P.; Piao, Y.; Lee, J.; Jun, S. W.; Moon, W. K.; Choi, S. H.; Hyeon, T. Large-Scale Synthesis of Bioinert Tantalum Oxide Nanoparticles for X-ray Computed Tomography Imaging and Bimodal Image-Guided Sentinel Lymph Node Mapping. *J. Am. Chem. Soc.* **2011**, *133*, 5508–5515.
25. Hallouard, F.; Briançon, S.; Anton, N.; Li, X.; Vandamme, T. F.; Fessi, H. Iodinated Nano-Emulsions as Contrast Agents for Preclinical X-ray Imaging, Impact of the Free Surfactants on the Pharmacokinetics. *Eur. J. Pharm. Biopharm.* **2013**, *83*, 54–62.
26. Anton, N.; Vandamme, T. F. The Universality of Low-Energy Emulsification. *Int. J. Pharm.* **2009**, *377*, 142–147.
27. Nebuloni, L.; Kuhn, G. A.; Müller, R. A Comparative Analysis of Water-Soluble and Blood-Pool Contrast Agents for *In Vivo* Vascular Imaging with Micro-CT. *Acad. Radiol.* **2013**, *20*, 1247–1255.
28. Boll, H.; Nittka, S.; Doyon, F.; Neumaier, M.; Marx, A.; Kramer, M.; Groden, C.; Brockmann, M. A. Micro-CT Based Experimental Liver Imaging Using a Nanoparticulate Contrast Agent: A Longitudinal Study in Mice. *PLoS One* **2011**, *6*, e25692.
29. Church, R. J.; Wu, H.; Mosedale, M.; Sumner, S. J.; Pathmasiri, W.; Kurtz, C. L.; Pletcher, M. T.; Eaddy, J. S.; Pandher, K.; Singer, M.; Batheja, A.; Watkins, P. B.; Adkins, K.; Harrill, A. H. A Systems Biology Approach Utilizing a Mouse Diversity Panel Identifies Genetic Differences Influencing Isoniazid-Induced Microvesicular Steatosis. *Toxicol. Sci.* **2014**, *140*, 481–492.
30. Tarantino, G.; Savastano, S.; Capone, D.; Colao, A. Spleen: A New Role for an Old Player?. *World J. Gastroenterol.* **2011**, *17*, 3776–3784.
31. Klymchenko, A.; Roger, E.; Anton, N.; Anton, H.; Shulov, I.; Vermot, J.; Mely, Y.; Vandamme, T. F. Highly Lipophilic Fluorescent Dyes in Nano-Emulsions: Towards Bright Non-leaking Nano-Droplets. *RSC Adv.* **2012**, *2*, 11876–11886.
32. Szebeni, J.; Muggia, F. M.; Alving, C. R. Complement Activation by Cremophor El as a Possible Contributor to Hypersensitivity to Paclitaxel: An *In Vitro* Study. *J. Natl. Cancer Inst.* **1998**, *90*, 300–306.
33. Anton, N.; Benoit, J. P.; Saulnier, P. Design and Production of Nanoparticles Formulated from Nano-Emulsion Templates—A Review. *J. Controlled Release* **2008**, *128*, 185–199.
34. Anton, N.; Gayet, P.; Benoit, J. P.; Saulnier, P. Nano-Emulsions and Nanocapsules by the Pit Method: An Investigation on the Role of the Temperature Cycling on the Emulsion Phase Inversion. *Int. J. Pharm.* **2007**, *344*, 44–52.
35. Anton, N.; Vandamme, T. F. Nano-Emulsions and Micro-emulsions: Clarifications of the Critical Differences. *Pharm. Res.* **2011**, *28*, 978–985.
36. Raschke, W. C.; Baird, S.; Ralph, P.; Nakoinz, I. Functional Macrophage Cell Lines Transformed by Abelson Leukemia Virus. *Cell* **1978**, *15*, 261–267.
37. Albanese, A.; Walkey, C. D.; Olsen, J. B.; Guo, H.; Emili, A.; Chan, W. C. Secreted Biomolecules Alter the Biological Identity and Cellular Interactions of Nanoparticles. *ACS Nano* **2014**, *8*, 5515–5526.
38. Guo, L.; Panderi, I.; Yan, D. D.; Szulak, K.; Li, Y.; Chen, Y. T.; Ma, H.; Niesen, D. B.; Seeram, N.; Ahmed, A.; Yan, B.; Pantazatos, D.; Lu, W. A Comparative Study of Hollow Copper Sulfide Nanoparticles and Hollow Gold Nanospheres on Degradability and Toxicity. *ACS Nano* **2013**, *7*, 8780–8793.
39. Herd, H.; Daum, N.; Jones, A. T.; Huwer, H.; Ghandehari, H.; Lehr, C. M. Nanoparticle Geometry and Surface Orientation Influence Mode of Cellular Uptake. *ACS Nano* **2013**, *7*, 1961–1973.